01 Nov 2018

Prediction of Thermal Conductance at Liquid-Gas Interfaces using Molecular Dynamics Simulations

James Gonzalez

Josue Ortega

Zhi Liang
Missouri University of Science and Technology, zlch5@mst.edu

Recommended Citation

J. Gonzalez et al., "Prediction of Thermal Conductance at Liquid-Gas Interfaces using Molecular Dynamics Simulations," *International Journal of Heat and Mass Transfer*, vol. 126, pp. 1183 - 1192, Elsevier, Nov 2018.
The definitive version is available at https://doi.org/10.1016/j.ijheatmasstransfer.2018.06.088

International Journal of Heat and Mass Transfer 126 (2018) 1183–1192

Contents lists available at ScienceDirect

International Journal of Heat and Mass Transfer

journal homepage: www.elsevier.com/locate/ijhmt

Prediction of thermal conductance at liquid-gas interfaces using molecular dynamics simulations

James Gonzalez, Josue Ortega, Zhi Liang *

Department of Mechanical Engineering, California State University, Fresno, Fresno, CA 93740, USA

ARTICLE INFO

Article history:
Received 2 May 2018
Received in revised form 14 June 2018
Accepted 17 June 2018
Available online 26 June 2018

ABSTRACT

Using molecular dynamics (MD) simulations and theoretical calculations, we study heat transfer across liquid-gas interfaces within a planar heat pipe. To determine the thermal conductance (Kapitza conductance), G_K, at the interface, two heat transfer mechanisms, namely, conduction and evaporation/condensation are considered. In the case of interfacial heat conduction, gas molecules, particularly non-condensable gas molecules, exchange heat with liquid surfaces through gas-liquid collisions, and the theoretical expression for G_K is derived from the kinetic theory of gases. For interfacial heat transfer by evaporation or condensation, the theoretical expression for G_K is derived from the Schrage relationships. To assess the accuracies of the theoretical expressions for G_K, we compare these theoretical predictions to the G_K obtained directly from MD simulations. For all cases studied, the theoretical predictions agree with the MD simulation results very well. If the density of non-condensable gas in the heat pipe is much higher than that of the working fluid in the gas phase, we find that the interfacial heat conduction could contribute significantly to the total heat flux across the liquid-gas interfaces. The effect of G_K at liquid-gas interfaces on the overall heat transfer efficiency in a planar heat pipe is discussed.

1. Introduction

Due to the existence of interfacial thermal resistance (Kapitza resistance) [1] R_K, heat flow across material interfaces can result in a discontinuous temperature drop at the interface. Since the thermal resistance at the interface between helium and a solid was first reported by Kapitza [2], R_K at a variety of solid-solid, solid-liquid, and solid-gas interfaces have been extensively studied by experiments, theoretical calculations, and numerical simulations [3–5]. Similarly, heat flow across a liquid-gas interface can also result in a temperature drop at the interface [6,7]. The ability to accurately predict R_K (or its inverse G_K) at liquid-gas interfaces is important for the thermal analysis of various types of heat pipes [8] and evaporation of liquid droplets [6]. For example, heat transfer efficiency in micro/nanoscale heat pipes is strongly limited by the R_K at liquid-gas interfaces [8]. A good understanding of heat transfer mechanisms at liquid-gas interfaces can help design heat pipes with optimized cooling performance.

In spite of its importance, the studies on R_K at liquid-gas interfaces are rare. One of the difficulties in the determination of R_K at liquid-gas interfaces is that the heat transfer across a liquid-gas interface often accompanies evaporation or condensation processes. Therefore, two heat transfer mechanisms, namely, conduction and evaporation/condensation should be considered in the analysis of heat transfer across liquid-gas interfaces. For heat transfer across solid-solid, solid-liquid, and solid-gas interfaces, only heat conduction needs to be considered in most cases.

The heat conduction at liquid-gas interfaces is due to collisions between gas molecules and liquid surfaces. Such a heat transfer mechanism is similar to that at solid-gas interfaces. The R_K at solid-gas interfaces is well predicted by theoretical expressions derived from the kinetic theory of gases [9–12]. Hence, we will employ these theoretical expressions to study conduction resistance at liquid-gas interfaces. Evaporation and condensation are processes by which a fluid transitions between its liquid state and its gas state at the liquid-gas interface. Recent molecular dynamics (MD) simulation results [8,13,14] show that the Schrage relationships [15,16] give an excellent prediction of the evaporation/condensation rates. Therefore, we will use theoretical expressions derived from the Schrage relationships to predict the evaporation/condensation thermal resistance at liquid-gas interfaces. Evaporation and condensation often occur when there is a non-condensable gas (NCG) in the gas phase, e.g. water evaporation/condensation in air. In this case, thermal energy can be transferred across the liquid-gas interface by both conduction (i.e., collisions between NCG molecules and liquid surfaces) and evaporation/condensation (i.e., liquid-vapor phase change of the

* Corresponding author.
E-mail address: zliang@csufresno.edu (Z. Liang).

https://doi.org/10.1016/j.ijheatmasstransfer.2018.06.088
0017-9310/

working fluid at the interface). In our previous MD studies [8,13], the heat transfer by conduction at the liquid-gas interface is neglected in the thermal analysis of the steady-state evaporation and condensation processes. In this work we take into account both conduction resistance and evaporation/condensation resistance at the liquid-gas interface, and investigate the contribution of conduction to the overall heat flow during evaporation/condensation processes.

In the next section, we will introduce the theory for thermal transport across a liquid-gas interface and the theoretical expressions for conduction resistance and evaporation/condensation resistance at liquid-gas interfaces. To assess the accuracies of the theoretical expressions, we will compare these theoretical predictions with the R_K obtained directly from MD simulations, which require no assumptions concerning the heat transfer mechanism at the liquid-gas interface. In Section 3 we describe the MD model for the study of heat transfer across liquid-gas interfaces, and the basic properties of the model fluid. In Section 4 we present MD simulation results, and discuss how the R_K at liquid-gas interfaces affect the heat transfer efficiency in planar heat pipes. Finally, we close with a summary and conclusions.

2. Theory

The interfacial thermal conductance (or Kapitza conductance), G_K, is defined as the ratio of heat flux across the interface to the temperature drop, ΔT, at the interface [1]:

$$G_K = q/\Delta T. \tag{1}$$

where the subscript K stands for Kapitza. Depending on the heat transfer mechanism, different theoretical expressions can be used to predict G_K at a liquid-gas interface.

2.1. Interfacial heat transfer by conduction

In the case of heat conduction across liquid-gas interfaces, there is no net mass flux at the interface, and gas molecules exchange thermal energies with liquid surfaces through gas-liquid collisions/interactions. The kinetic theory of gases predicts that the conduction resistance, $R_{K,cond}$, at liquid-gas interfaces is determined by the frequency of collisions between gas molecules and the liquid surface, and the efficiency of the thermal energy exchange during the liquid-gas collision process [9]. For incident gas molecules with an average temperature, T_g, and a density, ρ_g, the liquid-gas collision rate per area, N_g, is given by [9]:

$$N_g = \rho_g v_n = \rho_g \sqrt{RT_g/2\pi M_g}, \tag{2}$$

where v_n is the average normal velocity of incident gas molecules, M_g is the molar mass of gas molecules, and R is the gas constant. The heat exchange efficiency at a liquid-gas interface can be quantified by the thermal accommodation coefficient (TAC). For monoatomic gases, the TAC, α_T, is defined by [17]:

$$\alpha_T = \frac{T_r - T_i}{T_L - T_i}, \tag{3}$$

where T_i and T_r are the temperatures of incident and reflected gas molecules, respectively, and T_L is the liquid surface temperature. Theoretically, the TAC may vary between 0 (implying no energy transfer between the liquid and gas upon reflection) and 1 (characterizing diffuse reemission with complete thermal equilibration of the incident gas molecules with liquid). The TAC, α_T, and the collision rate, N_g, are related to the $G_{K,cond}$ (i.e., the inverse of $R_{K,cond}$) at liquid-gas interface by [9]:

$$G_{K,cond} = fRN_g \frac{\alpha_T}{2-\alpha_T}. \tag{4}$$

where $f = 4$ for a monatomic gas. Although Eq. (4) has been shown to give very good predictions of G_K at solid-gas interfaces [10,11], whether it is accurate or even valid in the prediction of G_K at liquid-gas interfaces remains debatable. In this work, we will test the validity and accuracy of Eq. (4) using MD simulations.

2.2. Interfacial heat transfer by evaporation/condensation

When evaporation/condensation occurs, energy is transferred by liquid-vapor phase changes at the interface. In this case, the interfacial heat flux, q, equals Jh_{fg}, where J is the evaporation/condensation rate, and h_{fg} is the latent heat. Recent MD simulations of steady state evaporation and condensation processes showed that the Schrage relationships, which were developed based on the kinetic theory of gases, accurately predict the evaporation/condensation rate, J [8,13,14]. Both the Schrage analysis and MD simulations of evaporation and condensation processes in a planar heat pipe (see Fig. 1) show that J is proportional to the temperature

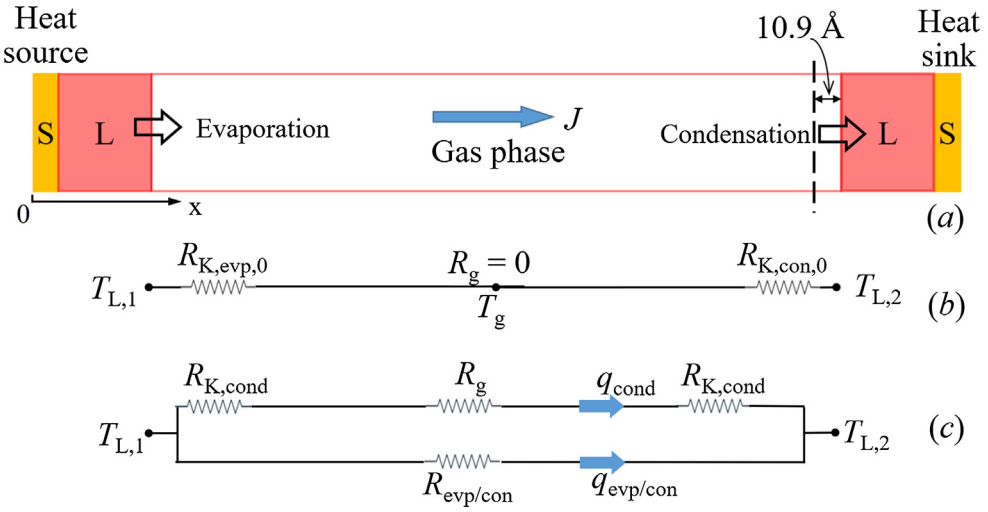

Fig. 1. (a) Schematic diagram of the model system for the study of evaporation and condensation in a planar heat pipe. S and L stand for the solid surface and the liquid phase, respectively. The vertical dashed line indicates the location of the imaginary plane (10.9 Å away from the liquid surface) for the determination of MAC. (b) The thermal resistance network between the evaporating and condensing interfaces in the heat pipe in the case of $\rho_{NCG} = 0$. (c) The thermal resistance network between the evaporating and condensing interfaces when an NCG is present in the heat pipe.

difference, $\Delta T_L = T_{L,1} - T_{L,2}$, between the evaporating and condensing liquid surfaces in the heat pipe [13,14] when ΔT_L is small. Accordingly, one can use the product of the proportionality constant, $J/\Delta T_L$, and h_{fg} to define the evaporation/condensation thermal conductance, $G_{evp/con}$, between the evaporating and condensing surfaces in the heat pipe. When the heat pipe only contains a pure (working) fluid, our recent theoretical analysis based on the Schrage relationships predicts [13]:

$$G_{evp/con,0} = \frac{\alpha_M}{2-\alpha_M}\sqrt{\frac{R}{2\pi M\bar{T}}}\left(\frac{\bar{T}}{\rho_{sat}}\frac{d\rho_{sat}}{dT}\bigg|_{\bar{T}} + \frac{1}{2}\right)\rho_{sat}h_{fg}, \tag{5}$$

where the subscript 0 indicates that the density of non-condensable (inert gas) equals zero in the heat pipe, $\bar{T}$ is the average temperature of the evaporating and condensing liquid surfaces in the heat pipe, M stands for molar mass of the working fluid, and ρ_{sat} is the saturated vapor density of the working fluid at temperature $\bar{T}$. In Eq. (5), α_M is the mass accommodation coefficient (MAC), which is defined as the fraction of vapor molecules that strike the liquid surface and are accommodated to the liquid phase. If the vapor phase of the working fluid is approximated as an ideal gas, an alternative form of $G_{evp/con,0}$ is [13,16]:

$$G_{evp/con,0} = \frac{\alpha_M}{2-\alpha_M}\sqrt{\frac{R}{2\pi M\bar{T}}}\left(\frac{h_{fg}}{R\bar{T}} - \frac{1}{2}\right)\rho_{sat}h_{fg}. \tag{6}$$

In deriving Eqs. (5) and (6), we did not make the assumption that the working fluid is a monatomic fluid [13]. Hence, we expect these expressions for thermal conductance are general. The inverse of $G_{evp/con,0}$ is the evaporation/condensation thermal resistance, $R_{evp/con,0}$, between the evaporating and condensing surfaces in the heat pipe, which is equal to the sum of the thermal resistances at the two liquid-gas interfaces and the thermal resistance in the gas phase (see Fig. 1(b)). During the steady state evaporation and condensation of a pure fluid in a heat pipe, the thermal resistance in the gas phase, R_g, is essentially zero, and the transport of thermal energy in the gas phase is through the bulk motion of the gas, rather than diffusive processes [13]. Since $R_g = 0$, the thermal resistance at each liquid-gas interface should be approximately $\frac{1}{2}R_{evp/con,0}$ if we assume the resistance at the evaporating surface is the almost same as that at the condensing surface. This assumption should be valid when the temperature difference between the two surfaces is small, which is the case in this study. Accordingly, the thermal conductance at the liquid-gas interface during the evaporation and condensation of a pure fluid is given by:

$$G_{K,evp/con,0} = 2G_{evp/con,0}. \tag{7}$$

The heat transfer via phase change is usually much more efficient than that by conduction. Therefore, we expect that $G_{K,evp/con,0}$ is much greater than $G_{K,cond}$ for the same fluid at the same temperature.

2.3. Interfacial heat transfer by both conduction and evaporation/condensation

Eqs. (4) and (7) provide theoretical expressions for liquid-gas interfacial thermal conductance when the interfacial heat transfer is by conduction or evaporation/condensation only. If a non-condensable gas (NCG) is present in the gas phase during the evaporation/condensation process, the interfacial heat transfer can be achieved by both evaporation/condensation of the working fluid, and collisions between the NCG molecules and liquid surfaces (i.e., interfacial heat conduction).

According to Eqs. (2) and (4), a higher density of NCG will result in a higher collision rate, which in turn will increase $G_{K,cond}$ at the liquid-gas interface. On the other hand, the presence of an NCG in a heat pipe can lead to diffusive mass transfer in the gas phase [8], which in turn reduces the evaporation/condensation rates. When the effect of NCG on evaporation and condensation of the working fluid is taken into account, our recent work [8] shows the evaporation/condensation thermal conductance between the evaporating and condensing surfaces in the heat pipe is given by:

$$G_{evp/con} = \frac{G_{evp/con,0}}{1 + \frac{\alpha_M}{2-\alpha_M}\sqrt{\frac{R\bar{T}}{2\pi M}}\frac{\rho_{NCG}L_g}{\rho_{tot}D_{AB}}}, \tag{8}$$

where ρ_{NCG} and ρ_{tot} are the density of NCG at the center of the gas phase and the total density of the gas mixture in the gas phase, respectively. L_g in Eq. (8) is the length of gas region in the heat pipe, and D_{AB} is the Maxwell-Stefan diffusion coefficient of the working fluid in the gas mixture. According to Eq. (8), $G_{evp/con}$ increases with decreasing ρ_{NCG}, and reaches its maximum value of $G_{evp/con,0}$ when $\rho_{NCG} = 0$ (i.e., evaporation/condensation of a pure working fluid).

When an NCG is present in a heat pipe shown in Fig. 1, both the bulk motion of the gas and diffusive heat transfer contribute to energy transport in the gas phase. As a result, there is a finite conduction resistance in the gas phase, which will lead to a finite temperature gradient in the gas region. Since there are temperature drops at the two liquid-gas interfaces, as well as in the gas region in this case, the evaporation/condensation conductance, $G_{K,evp/con}$, at each liquid-gas interface is not simply $2G_{evp/con}$. As shown in Fig. 1(c), it is more convenient to use $G_{evp/con}$ (i.e., the expression in Eq. (8)) directly rather than splitting $G_{evp/con}$ into the interfacial part and the bulk part in the thermal analysis of heat pipes containing an NCG. As ρ_{NCG} increases, the contribution from heat conduction to the total heat transfer rate in the heat pipe increases, and the contribution from the heat transfer by evaporation/condensation decreases. If the density of the NCG is much higher than that of the working fluid in the gas phase, then the contribution from heat conduction could be comparable to that from evaporation and condensation in the heat pipe.

In the following sections, we will use MD simulations to study the heat transfer across liquid-gas interfaces within a planar heat pipe, and assess the accuracies of the aforementioned theoretical expressions by comparing their predictions to MD simulation results.

3. MD simulation of heat transfer at liquid-gas interfaces

3.1. The MD model

In the MD model, we select fluid Ar as the working fluid and gas Ne as an NCG to study heat transfer across the liquid-gas interface in a planar heat pipe. Note that in a real heat pipe there is a return of condensed liquid to the evaporation region by, for example, capillary action. We do not consider this process in our MD model. As depicted in Fig. 1, the model planar heat pipe consists of two solid Au slabs. Each Au slab is formed by three (0 0 1) orientated Au atomic layers with a cross section area of 7.75 nm by 7.75 nm. The atoms in the outmost Au layers are fixed in the simulation. On each of two inner surfaces of Au slabs, we place a liquid Ar thin film. The initial thickness of the liquid Ar thin films on the left and right Au surfaces are 7 nm and 4.5 nm, respectively, such that the disjoining pressure has negligible effects on equilibrium properties of fluid Ar [14]. The gas region between the two liquid Ar surfaces has a length of $L_g = 106$ nm. To generate a heat flux across the liquid-gas interface, we carry out non-equilibrium MD (NEMD) simulations by setting the left Au slab as the heat source, and the right Au slab as the heat sink. As shown in Fig. 1, this results in evaporation at the left liquid-gas interface and condensation at the right liquid-gas interface. For comparison, we use a similar model system depicted in Fig. 2 to study heat conduction at the liquid-gas interface. To prevent evaporation and condensation,

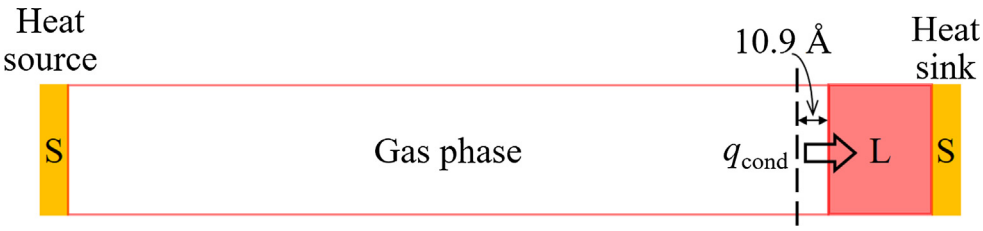

Fig. 2. Schematic diagram of the model system for the study of heat conduction across a liquid-gas interface. The vertical dashed line indicates the location of the imaginary plane (10.9 Å away from the liquid surface) for the determination of TAC.

we place a 6-nm-thick liquid Ar film only on the right Au surface, and set the left and right Au slabs as the heat source and heat sink, respectively. The length of the gas region between the left Au surface and the liquid Ar surface is ~70 nm. In this case, the heat transfer across the liquid-gas interface at steady state is by conduction only. To study the effect of NCG on heat transfer across the liquid-gas interface, we will gradually increase the density of NCG Ne in the gas region from 0 to 0.65 mol/L.

In all NEMD simulations the heat flows along the x direction, and periodic boundary conditions are applied in the y and z directions. The embedded-atom-method (EAM) potential [18] is used for Au-Au interactions. The Lennard-Jones (LJ) potential [19] is employed for all fluid-fluid and fluid-solid interactions. The LJ parameters [19,20] used in the simulation are summarized in Table 1. The cutoff distance for all LJ interactions is 10.9 Å. A relatively small Ar-Ne interaction strength is used to reduce the solubility of Ne in Ar, so that the small amount of Ne gas dissolved in liquid Ar has negligible effects on equilibrium properties of Ar [8].

A velocity Verlet algorithm [21] with a time step size of 5 fs is used to integrate the equations of motions. In NEMD simulations, the heat source temperature, T_h, and the heat sink temperature, T_l, are maintained by velocity rescaling [22] at each time step. Each heat source-sink simulation run is first carried for 10 ns to allow the system to reach quasi-steady state evaporation and condensation in the model system shown in Fig. 1, and steady state heat conduction in the model system shown in Fig. 2. We consider the evaporation/condensation process in the heat pipe as quasi-steady state since the liquid-gas interfaces move at a very low speed (less than 0.06 m/s in this study) as a result of the finite mass flux across the interface. The heat source-sink simulation run is then carried for an additional 20 ns for data collection and averaging. In the production run, we will calculate the temperature and density profiles in the liquid and gas phases. The contribution from non-zero bulk velocity is subtracted in the calculation of the temperature profile in the gas phase when evaporation/condensation occurs. The heat flux across the liquid-gas interface is obtained by determining the average heat fluxes added to the hot Au plate (q_h), and the average heat flux removed from the cold Au plate (q_l) at steady state. In each case of MD simulations, eight independent runs (i.e., eight different random seeds used to initialize atomic velocities) are performed to improve the accuracy of the simulation results. The uncertainties of the simulation results are determined by analyses of those independent runs and the propagation of uncertainties.

With the temperature profile and heat flux obtained from MD simulations, one can determine G_K at the liquid-gas interface directly from Eq. (1). All G_K's determined from MD simulations are evaluated at a temperature of 76 K in this work. The MD simulation results will be used to validate or assess the accuracy of the predictions from theoretical expressions given in Section 2. To evaluate these theoretical predictions, we use separate equilibrium and non-equilibrium MD simulations described in Section 3.2 through Section 3.5 to determine ρ_{sat}, h_{fg}, α_T, α_M, and D_{AB} for the model fluid, which are important parameters for theoretical expressions in Eq. (2) through Eq. (8).

Table 1
The LJ parameters used in the MD simulations. The Lorentz-Berthelot mixing rule is employed to calculate σ for Ar-Ne interactions.

	Ar-Ar [19]	Ne-Ne [19]	Ar-Ne	Ar-Au	Ne-Au
ε (meV)	10.3	4.04	4.04	10.3	4.04
σ (Å)	3.41	2.72	3.065	3.17 [20]	3.17

3.2. Determination of saturated vapor density and latent heat

The saturated vapor density, ρ_{sat}, and latent heat, h_{fg}, of the model fluid Ar are important fluid properties for the thermal analysis of the evaporation and condensation processes in the model system. To determine ρ_{sat}, we use the model system shown in Fig. 1(a) and equilibrate the whole system at a temperature of 76 K by maintaining both T_h and T_l at 76 K for 10 ns. After the system reaches the equilibrium, ρ_{sat} is determined from the average density of vapor Ar in the central gas region ranging from 20 to 100 nm in the model system. At T = 76 K, we obtain ρ_{sat} = 0.0695 ± 0.0006 mol/L. The MD simulation results show that the presence of the non-condensable gas Ne has little influence on the value of ρ_{sat} in the range of ρ_{NCG} simulated. Using separate equilibrium MD simulations, we further determine the internal energy, u, and pressure, P, of the saturated liquid Ar and saturated vapor Ar at the given temperature. Using the calculated u, P, and ρ, we determine the enthalpy of saturated liquid and vapor Ar. The difference between the two enthalpies gives h_{fg} = 6.30 ± 0.08 kJ/mol for the model fluid Ar at T = 76 K.

3.3. Determination of mass accommodation coefficient

The evaporation and condensation heat flux is affected by the mass accommodation coefficient (MAC), α_M, which is defined as the fraction of vapor molecules that strike the liquid surface, and are accommodated to the liquid phase. To determine α_M of the model fluid, we use the equilibrated system described in Section 3.2. We define the liquid-gas interface at the location where the average fluid density equals half of that in the liquid. As shown in Fig. 1(a), we set an imaginary plane 10.9 Å (cutoff distance) away from the liquid-vapor interface, and define the vapor Ar molecules that pass through the imaginary plane and move towards the interface as incident molecules. We follow the trajectory of each incident Ar molecule to determine the time interval, Δt, for each incident molecule to pass through the imaginary plane again and return to the vapor phase. An equilibrium MD simulation is carried for 10 ns to determine the total number of incident Ar molecules, N_{inc}, and the total number of incident molecules that returned to the vapor phase, N_{ref}, within Δt. At T = 76 K, the average normal velocity of incident vapor Ar molecules, i.e. v_n in Eq. (2), equals 50.1 m/s. Accordingly, for incident molecules that were directly reflected by the interface, the average Δt is ~44 ps. Fig. 3 shows that N_{ref}/N_{inc} keeps increasing with Δt. If an incident Ar

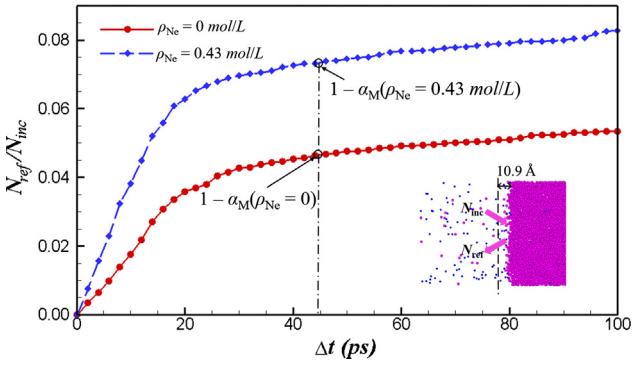

Fig. 3. The ratio of reflected to incident molecules, N_{ref}/N_{inc}, as a function of Δt at a temperature of 76 K when ρ_{Ne} = 0 and 0.43 mol/L. 1 − N_{ref}/N_{inc} at Δt = 44 ps is used to evaluate the MAC. The inset depicts a snapshot of fluid molecules near the interface and the position of the plane used to define N_{ref} and N_{inc}. The red and blue dots in the inset represent Ar and Ne atoms, respectively. The dashed and solid lines are used to guide the reader.

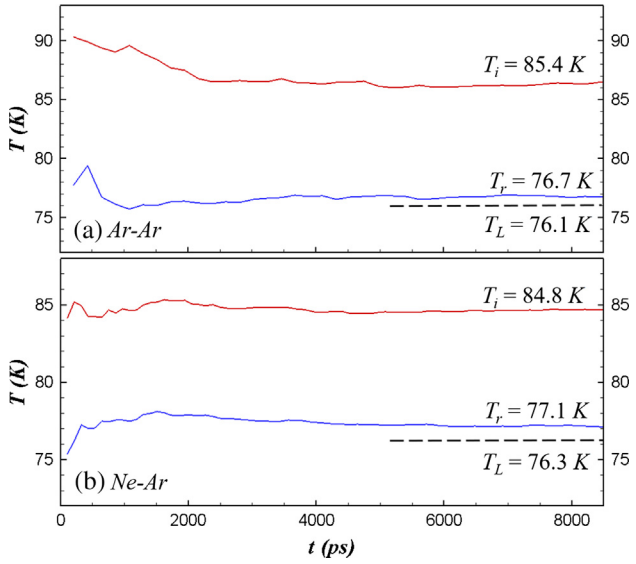

Fig. 4. The time-averaged temperature of incident, reflected gas molecules, and the liquid surface for (a) gas Ar on a liquid Ar surface, and (b) gas Ne on a liquid Ar surface.

molecule takes more than 44 ps to return to the vapor phase at T = 76 K, we consider that the Ar molecule is first accommodated to the liquid phase and later evaporated. As shown in Fig. 3, therefore, we use $\alpha_M = 1 - N_{ref}/N_{inc}$ at Δt = 44 ps to evaluate the MAC at T = 76 K. We used the same EMD method in our previous work [8,13] to evaluate the MAC of fluid Ar at various temperatures, and found the calculated MACs are consistent with values determined from the NEMD method in other literature.

The value of MAC is also affected by the density of NCG. As ρ_{NCG} increases, the possibility of collisions between incident Ar molecules and the Ne molecules near the liquid-vapor interface increases, which leads to a higher possibility of reflection. As shown in Fig. 3, N_{ref}/N_{inc} increases when an NCG is present in the gas phase, and as a result, the value of MAC decreases. The MD simulation results of α_M as a function of ρ_{NCG} are summarized in Table 2.

3.4. Determination of thermal accommodation coefficient

The thermal accommodation coefficient (TAC), α_T, is an important physical quantity for understanding the heat conduction at liquid-gas interfaces. In the model system shown in Fig. 2, we add gas Ne at a density of 0.17 mol/L to the gas phase and set T_h = 95 K to the left Au slab and T_l = 76 K to the right Au slab. At steady state, heat is transported across the liquid-gas interface by conduction. The resulting gas phase is a Ne-Ar gas mixture. To determine TAC of gas Ar and Ne on a liquid Ar surface using Eq. (3), we set an imaginary plane 10.9 Å (cutoff distance) away from the liquid-gas interface as shown in Fig. 2. The incident (or reflected) gas molecules pass through the imaginary plane indicating the start (or finish) of the heat exchange process. The temperature of incident (or reflected) gas Ar and gas Ne molecules is obtained by dividing the average kinetic energy of the incident (or reflected) Ar and Ne molecules by $2k_B$ [9]. The time-averaged T_i, T_r, and T_L obtained from the aforementioned NEMD simulations are shown in Fig. 4. According to the definition of TAC in Eq. (3), the MD simulation results predict that $\alpha_T = 0.94 \pm 0.01$ for gas Ar on a liquid Ar surface, and $\alpha_T = 0.90 \pm 0.01$ for gas Ne on a liquid Ar surface.

We used the same method in our previous work to determine TAC at solid surfaces and found that the TAC gets higher on a softer surface [12]. The liquid Ar surface in the model system can be considered as an ultrasoft solid surface, which implies a high TAC value. Moreover, Fig. 3 shows most of incident gas Ar molecules (>90%) are accommodated to the liquid phase for more than 100 ps before being evaporated back to the gas phase. Hence, the majority of incident Ar molecules have enough time to thermalize with the liquid phase before returning to the gas phase. This explains the close to unity α_T for gas Ar on a liquid Ar surface obtained from the MD simulation. Our previous MD study [12] on TAC also showed that the TAC value decreases as the mass mismatch between gas and surface atoms increases. The gas-liquid atomic mass ratio for gas Ar on a liquid Ar surface and gas Ne on a liquid Ar surface are 1.0 and 0.51, respectively. The greater mass mismatch between Ne and Ar molecules is consistent with the slightly lower α_T for gas Ne on a liquid Ar surface that was found in the MD simulation.

3.5. Determination of the diffusion coefficient and thermal conductivity in the gas phase

The Maxwell-Stefan diffusion coefficient, D_{AB}, and thermal conductivity, k_g, of the Ar-Ne gas mixture are important parameters

Table 2
MD simulation results of α_M, α_T, $\rho_{tot}D_{AB}$, and k_g as a function of ρ_{Ne}. The total thermal conductance, G_{tot}, between the evaporating and condensing surface in the model heat pipe as a function of ρ_{Ne}, determined by theoretical calculations and MD simulations. The last column shows the percentage contribution from G_{cond} to G_{tot}.

ρ_{Ne} (mol/l)	α_M	α_T (Ne-Ar)	$\rho_{tot}D_{AB}$ (mol/m s)	k_g (W/m K)	G_{tot} (MW/m^2 K)		$G_{cond.}/G_{tot}$ (%)
					Theory	MD	
0.00	0.95	–	–	–	2.48 ± 0.04	2.39 ± 0.07	0
0.20	0.95	0.90	0.49×10^{-3}	0.021	0.94 ± 0.02	0.96 ± 0.05	10.3
0.34	0.94	0.90	0.50×10^{-3}	0.022	0.70 ± 0.04	0.73 ± 0.04	18.1
0.49	0.93	0.90	0.51×10^{-3}	0.023	0.59 ± 0.02	0.60 ± 0.04	25.9
0.65	0.93	0.90	0.51×10^{-3}	0.023	0.51 ± 0.03	0.50 ± 0.03	31.6

that affect the diffusive heat and mass transfer in the gas region of the model heat pipe. Eq. (8) shows that the evaporation/condensation conductance at the liquid-gas interface is also affected by the diffusion coefficient, D_{AB}. Both D_{AB} and k_g of the model fluid can be determined by equilibrium MD simulations.

The results in Section 3.2 show that $\rho_{sat} \approx 0.07$ mol/L for the model fluid Ar at a temperature of 76 K. If gas Ne at a density of 0.20 mol/L is added to the saturated vapor Ar, the total density of the gas mixture, ρ_{tot}, is ~0.27 mol/L. To determine D_{AB} and k_g for this gas mixture, we place 16,384 atoms (74% Ne and 26% Ar) in a cubic simulation box. The box size is fixed at 46.4 nm during the MD simulation to maintain ρ_{tot} at 0.27 mol/L. After the gas mixture reaches the thermal equilibrium at $T = 76$ K, D_{AB} and k_g are determined from Green-Kubo formulas. The Green-Kubo formula for determining D_{AB} is given by [23]:

$$D_{AB} = \frac{y_{Ne}}{3N_{Ar}}\left(\frac{y_{Ar}m_{Ar} + y_{Ne}m_{Ne}}{y_{Ne}m_{Ne}}\right)^2 \int_0^\infty dt \left\langle \sum_{i=1}^{N_{Ar}} \vec{v}_{Ar}^{\,i}(0) \cdot \sum_{i=1}^{N_{Ar}} \vec{v}_{Ar}^{\,i}(t) \right\rangle, \tag{9}$$

where N_{Ar} is the number of Ar atoms in the Ar-Ne mixture, m_{Ar} and m_{Ne} are atomic mass of Ar and Ne, respectively, v_{Ar} is the velocity of Ar atoms, t is time. In Eq. (9), y_{Ar} and y_{Ne} are the mole fractions of Ar and Ne in the gas mixture, respectively. The Green-Kubo formula for determining k_g is given by [21]:

$$k_g = \frac{V}{3k_B T^2} \int_0^\infty \langle \vec{q}(t)\vec{q}(0)\rangle dt, \tag{10}$$

where V is the volume of the simulation box, k_B is the Boltzmann constant, and q is the microscopic heat flux, which can be computed from [24,25]:

$$\vec{q} = \frac{1}{V}\left[\sum_i E_i \vec{v}_i + \frac{1}{2}\sum_i \sum_j \vec{r}_{ij}(\vec{f}_{ij} \cdot \vec{v}_i)\right]. \tag{11}$$

In Eq. (11), v_i and E_i are the velocity and total energy of atom i, respectively, r_{ij} is the position vector from atom j to atom i, and f_{ij} is the interatomic force on atom i exerted from atom j. To obtain good statistics of the simulation results, 1 ms is used to calculate the velocity autocorrelation function (VACF) in Eq. (9), and the heat flux autocorrelation function (HFACF) in Eq. (11). In Fig. 5, we show VACF, HFACF, and their running integrals for the Ar-Ne gas mixture at $T = 76$ K and $\rho_{tot} = 0.27$ mol/L. From the plateau of the running integral, we evaluate $D_{AB} \approx 1.80 \times 10^{-6}$ m^2/s and $k_g \approx 0.021$ W/m K. Since $\rho_{tot} = 0.27$ mol/L, we obtain the product $\rho_{tot}D_{AB} = 0.49 \times 10^{-3}$ mol/m s.

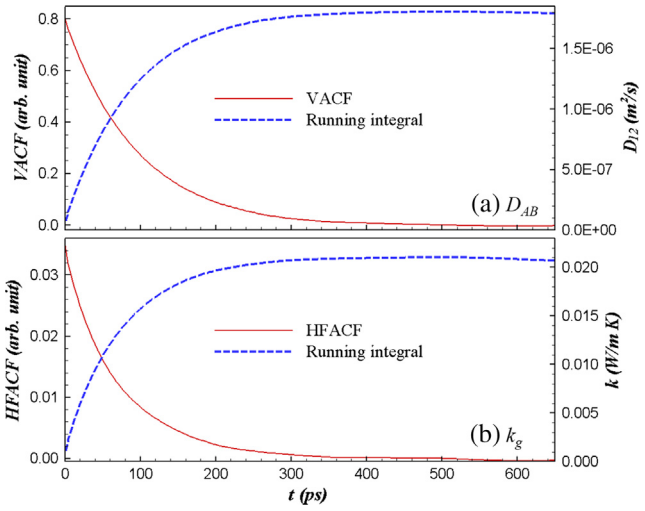

Fig. 5. (a) The VACF and its running integral, and (b) the HFACF and its running integral for the model Ar-Ne gas mixture at $T = 76$ K and $\rho_{tot} = 0.27$ mol/L.

To study the effect of NCG on heat transfer in the model heat pipe, we will gradually increase the density of gas Ne in the gas mixture to 0.65 mol/L. Using the same method, we calculate D_{AB} and k_g at $T = 76$ K, and ρ_{Ne} in the range of 0.20 –0.65 mol/L. In Table 2, we show the calculated $\rho_{tot}D_{AB}$ and k_g as a function of ρ_{Ne}. The kinetic theory of gases predicts that $\rho_{tot}D_{AB}$ should be independent of the mixture composition and ρ_{tot} for low-density gases [26]. The essentially constant $\rho_{tot}D_{AB}$ found from the MD simulation is consistent with the prediction from the kinetic theory of gases. Gas Ne is more thermally conductive than gas Ar at the same temperature. Hence, it is reasonable to see in Table 2 that the thermal conductivity of the mixture increases as the fraction of gas Ne in the Ar-Ne mixture increases.

4. NEMD simulation results

4.1. Heat conduction at the interface between liquid Ar and its own vapor

If the model fluid system only contains fluid Ar, the liquid-gas interface is formed by the liquid Ar and its own vapor. If no phase change occurs at the liquid-vapor interface, the thermal energy is transported across the interface by conduction only. We first use the model system shown in Fig. 2 to study heat conduction at the interface between liquid Ar and its own vapor. In this case, the theoretical prediction for $G_{K,cond}$ is given by Eq. (4). Its accuracy will be assessed by comparing it to the MD simulation result.

Fig. 6 shows the MD simulation results in the case of $T_h = 95$ K and $T_l = 76$ K. Since no liquid layer is present on the left high-temperature surface, evaporation will not take place at the left surface. Accordingly, no condensation will occur on the right low-temperature surface at steady state. Hence, there is no mass flux in the model system and the heat transfer is by conduction only. In the heat flow direction, the vapor temperature decreases (see Fig. 6(a)), which results in a slight increase in the vapor density (see inset of Fig. 6(b)). By extrapolating the linear fit to the temperature profiles in the liquid and gas phases to the liquid-gas interface, we see an evident temperature drop, $\Delta T = 5.4 \pm 0.1$ K, at the interface. In addition from the MD simulation, we obtain that $q_h \approx q_l = 0.55 \pm 0.01$ MW/m^2. Accordingly, the NEMD simulation predicts that $G_{K,MD} = 0.102 \pm 0.003$ MW/m^2 K.

To compare the MD simulation result with the theoretical expression from Eq. (4), we first find from Fig. 6 that the temperature and density of vapor Ar near the interface are $T_g = 81.5$ K and $\rho_g = 0.064$ mol/L, respectively. Using Eq. (2), we obtain the liquid-gas collision rate, $N_g = 3.32$ kmol/m^2 s. In Section 3.4, we already determined from MD simulations that $\alpha_T = 0.94 \pm 0.01$ for gas Ar on a liquid Ar surface. Substituting these properties into Eq. (4), we obtain the theoretical prediction $G_{K,cond} = 0.098 \pm 0.002$ MW/m^2 K, which agrees with $G_{K,MD} = 0.102 \pm 0.003$ MW/m^2 K very well.

4.2. Evaporation/condensation at the interface between liquid Ar and its own vapor

For comparison, we use the model system shown in Fig. 1(a) to determine the evaporation/condensation thermal conductance, $G_{K,evp/con,0}$, at the interface between liquid Ar and its own vapor. In the NEMD simulation, we set $T_h = 79$ K and $T_l = 73$ K such that the average temperature of the fluid in the model system is around 76 K. The temperature and density profiles during the quasi-steady state evaporation and condensation processes in the model system are shown in Fig. 7. The MD simulation results show the density

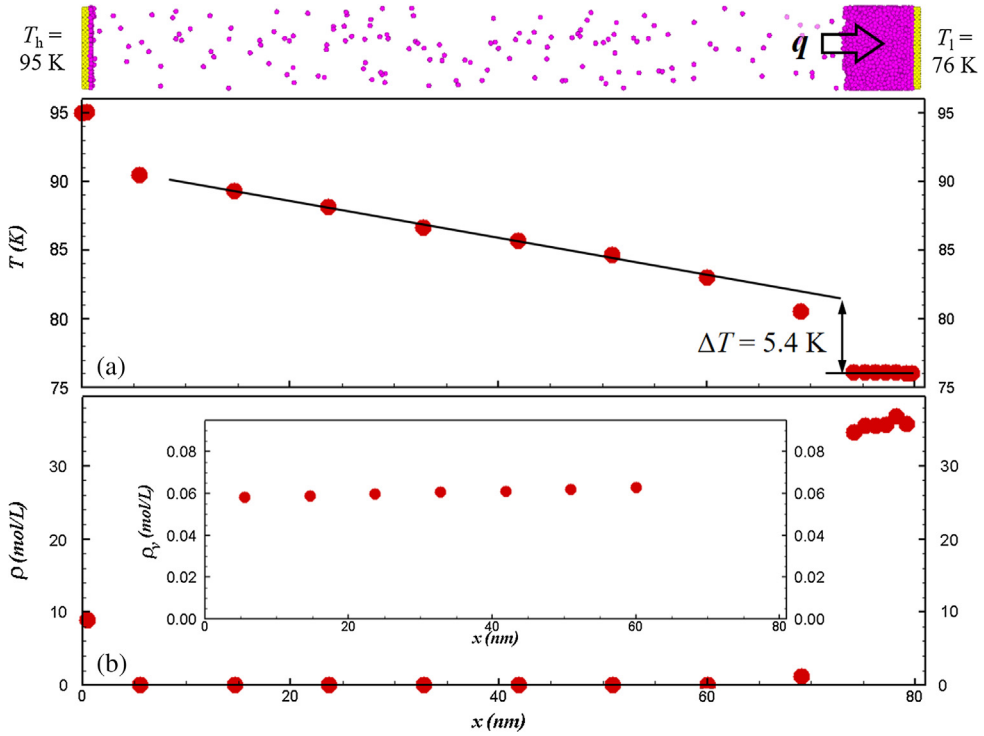

Fig. 6. (Top panel) A snapshot of the model system during the steady state heat conduction process in the case of T_h = 95 K and T_l = 76 K. (Bottom panels) Steady state (a) temperature, and (b) density profiles in the case of T_h = 95 K and T_l = 76 K. The straight lines in (a) show the linear fit to the temperature profile in the gas and liquid phases. The inset in (b) shows the density profile in the vapor phase.

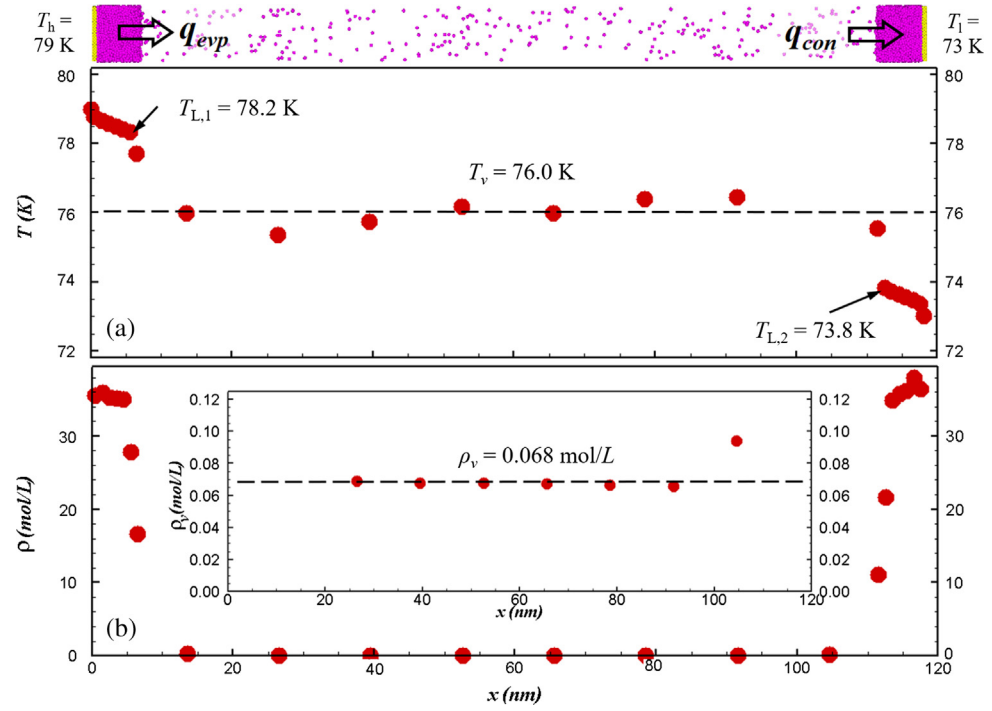

Fig. 7. (Top panel) A snapshot of the model system during the quasi-steady state evaporation and condensation processes in the case of T_h = 79 K and T_l = 73 K. (Bottom panels) Steady state (a) temperature, and (b) density profiles in the case of T_h = 79 K and T_l = 73 K. The dashed horizontal line in (a) indicates the average value of temperature in the central gas region. The statistical error of the temperature in the gas phase is ~0.3 K. The inset in (b) shows the density profile in the vapor phase.

and temperature gradients in the vapor phase are almost zero. This indicates that there is essentially no resistance to the heat and mass flow in the gas region. Therefore, the thermal resistance between the evaporating and condensing surfaces is only located at the two liquid-gas interfaces. This confirms the theoretical prediction given by Eq. (7).

To determine the interfacial thermal conductance, we first find the temperature at the left liquid surface $T_{L,1}$ = 78.2 K and that at the right liquid surface $T_{L,2}$ = 73.8 K as shown in Fig. 7(a). $T_{L,1}$ and $T_{L,2}$ are determined by linear extrapolating the temperature profile in the liquid film to the liquid-gas interface. Near the liquid-gas interface, there are strong non-equilibrium regions where the temperature of fluid can be anisotropic [26,27]. In the middle of the gas region, the vapor is close to the local equilibrium [13,26]. The temperature points near the interface are ignored in the linear fit to the temperature profile. Since the temperature in the middle of vapor phase is essentially a constant around 76 K, the temperature drops at the two liquid-gas interfaces are both around 2.2 K. Furthermore, from the MD simulation, we obtain that $q_h \approx q_l = 10.5 \pm 0.02$ MW/m^2, which indicates the evaporation and condensation heat fluxes are essentially the same at the two liquid surfaces. Using Eq. (1), we find $G_{K,MD} = 4.77 \pm 0.14$ MW/m^2 K at an interface between liquid Ar and its own vapor when evaporation/condensation occurs. This value is about 50 times greater than G_K at the same interface when interfacial heat transfer is by conduction only.

To compare $G_{K,MD}$ with the theoretical prediction given by Eqs. (6) and (7), we first find the average temperature of the evaporating and condensing liquid surfaces $\overline{T}$ = 76 K. In Section 3, we already determined from MD simulations that α_M = 0.95, ρ_{sat} = 0.0695 mol/L, and h_{fg} = 6.30 kJ/mol for the model fluid Ar at $\overline{T}$ = 76 K. Substituting these properties in Eq. (6), we obtain the total thermal conductance between the evaporating and condensing interfaces, $G_{evp/con,0}$, equals 2.48 ± 0.04 MW/m^2 K. Accordingly, the theoretical prediction of $G_{K,evp/con,0}$ on each of the two liquid-gas interfaces is 4.96 ± 0.08 MW/m^2 K, which is consistent with $G_{K,MD}$ = 4.77 ± 0.14 MW/m^2 K.

4.3. Heat conduction at the interface between liquid Ar and Ar-Ne gas mixture

To study the effect of NCG on interfacial heat transfer, we add gas Ne to the model system in Section 4.1. In this case, the gas phase is a mixture of gas Ne and vapor Ar, and there is no net evaporation and condensation at the liquid-gas interface. The heat transfer between the Ar-Ne gas mixture and the liquid Ar surface is by conduction only. To generate a heat flux across the liquid-gas interface, we set T_h = 95 K and T_l = 76 K in the MD simulation. At steady state, both gas Ne and vapor Ar exchange heat with the liquid surface through collisions between gas molecules and the liquid surface. Therefore, we can use Eq. (4) to predict the $G_{K,cond}$ at the interface between vapor Ar and liquid Ar, and the $G_{K,cond}$ at the interface between gas Ne and liquid Ar. The sum of these two $G_{K,cond}$'s gives the total $G_{K,cond}$ at the interface between the liquid Ar and the Ar-Ne gas mixture.

To determine the theoretical prediction, we first fit the temperature profile in the gas phase by a linear function as shown in Fig. 8 (a). By extrapolating the linear fit to the liquid-gas interface, we find T_g = 80.6 K at the interface. Additionally, we find from the density profile shown in Fig. 8(b) that the densities of gas Ne and vapor Ar near the liquid-gas interface are ρ_{Ne} = 0.177 mol/L and ρ_{Ar} = 0.0672 mol/L, respectively. Accordingly, Eq. (2) predicts that the liquid-gas collision rates for gas Ne and vapor Ar on the liquid surface are $N_{g,Ne}$ = 12.87 kmol/m^2 s and $N_{g,Ne}$ = 3.47 kmol/m^2 s, respectively. Moreover, we found in Section 3.4 that α_T = 0.94 for gas Ar on a liquid Ar surface, and α_T = 0.90 for gas Ne on a liquid Ar surface. Substituting the values of α_T and N_g into Eq. (4), we obtain the theoretical prediction of $G_{K,cond}$ for gas Ne and vapor Ar on the liquid Ar surface as 0.35 MW/m^2 K and 0.10 MW/m^2 K, respectively. Therefore, the theoretical prediction for the total $G_{K,cond}$ at the interface between liquid Ar and Ar-Ne gas mixture equals 0.45 ± 0.01 MW/m^2 K.

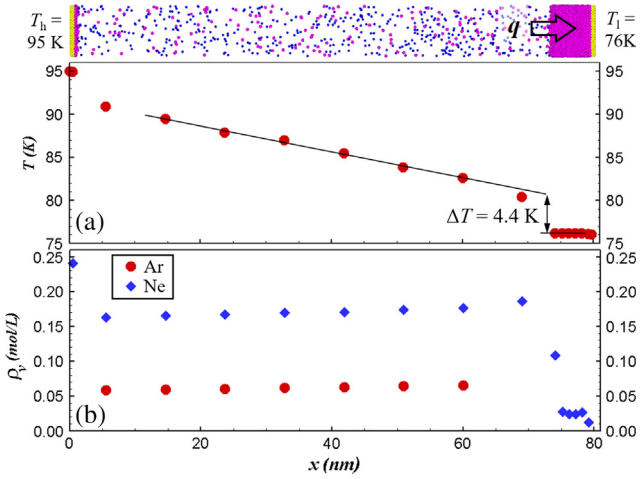

Fig. 8. (Top panel) A snapshot of the model system containing both fluid Ar and Ne during the steady state heat conduction process in the case of T_h = 95 K and T_l = 76 K. The blue dots in the snapshot represent Ne atoms. (Bottom panels) Steady state (a) temperature, (b) Ar density, and Ne density profiles in the case of T_h = 95 K and T_l = 76 K. The straight lines in (a) show the linear fit to the temperature profile in the gas and liquid phases.

To access the accuracy of the above theoretical prediction, we find the temperature drop, ΔT = 4.4 ± 0.2 K, at the liquid-gas interface from the steady-state temperature profile shown in Fig. 8(a). Furthermore, from the MD simulation, we obtain that $q_h \approx q_l$ = 2.03 ± 0.05 MW/m^2. Accordingly, the NEMD simulation predicts that $G_{K,MD}$ = 0.46 ± 0.02 MW/m^2 K, which is consistent with the theoretical prediction $G_{K,cond}$ = 0.45 ± 0.01 MW/m^2 K.

4.4. Heat transfer by both conduction and evaporation/condensation at the interface between liquid Ar and Ar-Ne gas mixture

The model system used in this section is similar to that in Section 4.2. The only difference is that a non-condensable gas Ne is added between the evaporating and condensing interfaces. Fig. 9 shows the representative MD simulation results in the case of T_h = 79 K, T_l = 73 K, and $\rho_{Ne} \approx$ 0.49 mol/L. Unlike the results shown in Fig. 7, we can see evident temperature and density gradients

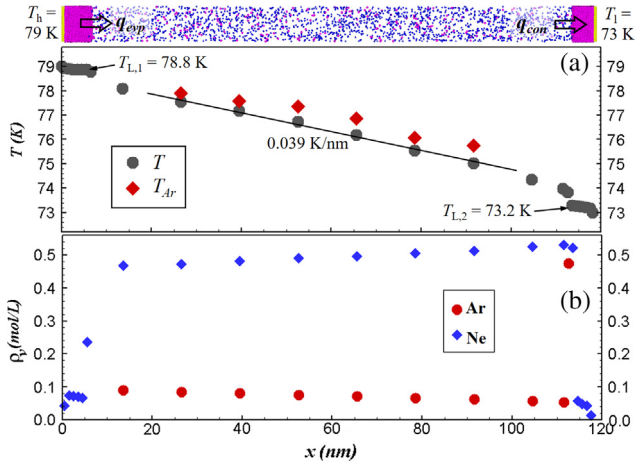

Fig. 9. (Top panel) A snapshot of the model system during the quasi-steady state evaporation and condensation processes in the case of T_h = 79 K, T_l = 73 K, and $\rho_{Ne} \approx$ 0.49 mol/L. The blue dots in the snapshot represent Ne atoms. (Bottom panels) Steady state (a) temperature, (b) Ar density, and Ne density profiles in the case of T_h = 79 K, T_l = 73 K, and $\rho_{Ne} \approx$ 0.49 mol/L. The solid line in (a) indicates a linear fit to the temperature in the central gas region. The diamond scatters in (a) represents Ar temperatures in the gas phase. The statistical error for T and T_{Ar} in the central gas region is ~0.1 K and ~0.3 K, respectively.

in the gas phase in Fig. 9. The non-zero gradients imply diffusive heat and mass transfer in the gas phase. In this case, the thermal energy can be transported from the evaporating liquid surface to the condensing surface by both conduction and bulk fluid motions. Although the heat conduction between the two interfaces is induced by the presence of the NCG Ne, the collisions between Ne and Ar atoms over a distance multiple times the mean free path of gas molecules also result in a temperature gradient in vapor Ar as shown in Fig. 9(a). According to our analysis in Section 2.3, the thermal resistance network between the two liquid-gas interfaces are shown in Fig. 1(c). To obtain the theoretical prediction of the total thermal resistance, R_{tot}, between the two interfaces, we need to find the conduction resistance, R_{cond}, and the evaporation/condensation resistance, $R_{evp/con}$ (i.e. the inverse of $G_{evp/con}$) between the two interfaces separately.

We first use Eq. (8) to calculate the evaporation/condensation resistance, $R_{evp/con}$. From Section 4.2, we determined $G_{evp/con,0}$ = 2.48 ± 0.04 MW/m^2 K for fluid Ar at $\overline{T}$ = 76 K. In the denominator of the expression in Eq. (8), $\rho_{NCG} \approx$ 0.49 mol/L and L_g = 106 nm. Furthermore, we found in Section 3.5 that $\rho_{tot}D_{AB} = 0.51 \times 10^{-3}$ mol/m s. With these values, Eq. (8) predicts $G_{evp/con}$ = 0.44 ± 0.01 MW/m^2 K ($R_{evp/con}$ = 2.27 ± 0.06 m^2 K/MW).

Secondly, we determine the theoretical prediction of R_{cond} between the two interfaces. The heat conduction at the liquid-gas interface in this case is due to the collisions between Ne gas molecules and the liquid Ar surface. To determine the $R_{K,cond}$ at the interface, we first calculate the collision rate, $N_{g,Ne}$, using Eq. (2). From Fig. 9, we find the temperature and density of gas Ne are about 76 K and 0.49 mol/L, respectively. Hence, $N_{g,Ne}$ is equal to 34.6 kmol/m^2 s. With the value of $N_{g,Ne}$ and $\alpha_{T,Ne}$ = 0.90 found in Section 3.4, Eq. (4) predicts $G_{K,cond}$ = 1.03 ± 0.02 MW/m^2 K ($R_{K,cond}$ = 0.97 ± 0.02 m^2 K/MW). The conduction resistance in the gas phase is $R_g = L_g/k_g$. For the Ar-Ne gas mixture at the given temperature, density, and composition, we found in Section 3.5 that k_g = 0.023 W/m K. Using L_g = 106 nm and k_g = 0.023 W/m K, we obtain R_g = 4.61 m^2 K/MW. It is shown in Fig. 1(c) that $R_{cond} = 2R_{K,cond} + R_g$. Accordingly, we find R_{cond} = 6.55 ± 0.05 m^2 K/MW (G_{cond} = 0.153 ± 0.002 MW/m^2 K).

Fig. 1(c) shows R_{cond} and $R_{evp/con}$ are in parallel arrangement. Hence, the theoretical prediction of R_{tot} between the two interfaces equals to 1.69 ± 0.02 m^2 K/MW. Accordingly, the G_{tot} (i.e. the inverse of R_{tot}) is equal to 0.59 ± 0.01 MW/m^2 K. To access the accuracy of the above theoretical prediction, we find from Fig. 9(a) that the temperature at the left and right liquid surfaces are $T_{L,1}$ = 78.8 K and $T_{L,2}$ = 73.2 K, respectively. We also find from MD simulation that $q_h \approx q_l$ = 3.30 ± 0.15 MW/m^2. Hence, the total thermal conductance between the two liquid surfaces predicted directly from the MD simulation is $G_{tot,MD} = q/(T_{L,1} - T_{L,2})$ = 0.59 ± 0.03 MW/m^2 K, which agrees with the theoretical prediction (0.59 ± 0.01 MW/m^2 K).

Using the temperature difference, $\Delta T_L = T_{L,1} - T_{L,2}$, and the theoretical prediction of the conduction resistance, R_{cond}, between the two interfaces, we further find that the conduction heat flux, $q_{cond} = \Delta T_L/R_{cond}$, between the two interfaces equals 0.86 ± 0.01 MW/m^2. This theoretical prediction can be compared with q_{cond} evaluated directly from the MD simulation. It is shown in Fig. 9(a) that the temperature gradient in the gas phase is ~0.039 K/nm. Using k_g = 0.023 W/m K found in Section 3.5, the q_{cond} predicted directly from the MD simulation is 0.90 ± 0.02 MW/m^2, which is again consistent with the theoretical prediction. This result indicates the evaporation/condensation heat flux, $q_{evp/con}$, is transported in the gas phase by bulk motions of Ar. The $q_{evp/con}$ will not result in a temperature gradient in the gas phase. If no NCG is present, q_{cond} will be zero and the temperature gradient in the gas phase will be zero as shown in Section 4.2.

Finally, by comparing G_{cond} with $G_{evp/con}$ in this representative simulation case, we find the contribution from the conduction heat transfer cannot be neglected, and q_{cond} between the two liquid-gas interfaces accounts for ~26% of the total heat flux. This result is caused by the much higher ρ_{Ne} as compared to ρ_{Ar} in the gas phase. According to the theoretical analysis in Section 2.3, as the density of NCG in the heat pipe increases, G_{cond} will increase and $G_{evp/con}$ will decrease. When we gradually increase ρ_{Ne} from 0 to 0.65 mol/L in our model system, the calculated G_{cond}/G_{tot} increases from 0 to 31.6% as shown in Table 2. These predictions indicate that G_{cond} can be comparable to $G_{evp/con}$ if the density of NCG is much higher than that of working fluid in the gas phase. We also show in Table 2 that the theoretical prediction of G_{tot} is in agreement with G_{tot} obtained directly from MD simulation in all simulated cases.

5. Discussions

The results in Section 4 showed that the theoretical expressions for liquid-gas interfacial thermal conductance are accurate. Hence, we will use these theoretical expressions to predict the effective thermal conductivity, k_{eff}, of the gas region within a planar heat pipe during the steady-state evaporation and condensation processes. In this case, k_{eff} is related to the total thermal conductance, G_{tot}, between the evaporating and condensing liquid surfaces by:

$$k_{eff} = L_g G_{tot}. \tag{12}$$

If no NCG is present in the heat pipe, $G_{tot} = G_{evp/con,0}$. Eq. (6) shows that at a given temperature $G_{evp/con,0}$ is a constant independent of L_g. Therefore, k_{eff} should be proportional to L_g in the absence of an NCG.

When an NCG is present in the heat pipe, $G_{tot} = G_{cond} + G_{evp/con}$, where $G_{cond} = 1/(2R_{K,cond} + L_g/k_g)$ and $G_{evp/con}$ is given by Eq. (8). Both G_{cond} and $G_{evp/con}$ decrease with increasing L_g. In the limit of large L_g, $G_{cond} \approx k_g/L_g$ and $G_{evp/con}$ is given by:

$$G_{evp/con} \approx \left(\frac{h_{fg}}{R\overline{T}} - \frac{1}{2}\right)\frac{\rho_{tot}D_{AB}}{\rho_{NCG}\overline{T}}\frac{\rho_{sat}h_{fg}}{L_g}. \tag{13}$$

Therefore, k_{eff} in the limit of large L_g is given by:

$$k_{eff} = \left(\frac{h_{fg}}{R\overline{T}} - \frac{1}{2}\right)\frac{\rho_{tot}D_{AB}}{\rho_{NCG}\overline{T}}\rho_{sat}h_{fg} + k_g. \tag{14}$$

This first term on right side of Eq. (14) is the contribution from heat transfer by evaporation/condensation. The second term is the contribution from heat conduction. As we showed in Section 4.4, for heat transfer in a nanoscale heat pipe, the contribution from heat conduction cannot be neglected if the density of the NCG is significantly higher than that of the working fluid in the gas phase. To see if the heat conduction also gives a non-negligible contribution to the heat transfer in a micro/macroscale heat pipe, we use Eq. (14) to calculate the k_{eff} in a heat pipe whose working fluid is water and the NCG is air at 1 atm. If the heat pipe is operating at an average temperature of 25 °C, using h_{fg} = 2442 kJ/kg [28], ρ_{sat} = 0.0231 kg/m^3 [28], $D_{AB} = 0.282 \times 10^{-4}$ m^2/s, [29] and $\rho_{tot} \approx \rho_{NCG}$, we obtain that the first term on right hand side of Eq. (14) equals 0.092 W/m K. At 1 atm and 25 °C, the second term on right hand side of Eq. (14), k_g, equals 0.026 W/m K [28]. Hence, Eq. (14) predicts that the k_{eff} = 0.118 W/m K in the gas phase, and ~22% of the total heat flux is due to the heat conduction in the gas phase. The non-negligible contribution from the heat conduction is caused by the very high air density as compared to the density of water vapor. As temperature increases, the density of water vapor in the heat pipe will increase rapidly. As a result, the k_g in Eq. (14) will become negligible at high temperatures, and the heat transfer between the two liquid surfaces will be dominated by

evaporation/condensation. Certainly, these predictions should be further validated in the future by independent MD simulations on water evaporation in air or by experiment.

6. Conclusions

The thermal energy can be transferred across the liquid-gas interface by both conduction and evaporation/condensation. The interfacial heat conduction is achieved by collisions between gas molecules and the liquid surface. The conduction resistance at the liquid-gas interface is determined by the liquid-gas collision rate and the TAC of gas molecules on the liquid surface. The MD simulation results show that Eq. (4), which was derived from the kinetic theory of gases, accurately predicts the conduction resistance at liquid-gas interfaces. When evaporation or condensation occurs, the evaporation/condensation resistance at the liquid-gas interface is well predicted by theoretical expressions derived from the Schrage relationships. While we expect that these theoretical expressions can be also used to predict the liquid-gas interfacial thermal conductance for complex fluids, the validity of these theoretical expressions should be tested in the future in systems with more complex fluids such as water or polymer evaporation/condensation in air.

The NCG present in the heat pipe plays two roles in heat transfer at liquid-gas interfaces. On one hand, both MD simulation results and theoretical predictions show that it reduces the evaporation/condensation heat and mass fluxes at the liquid-gas interface. On the other hand, it creates another channel (i.e. heat conduction) for heat transfer across the interface. If the density of the NCG is much higher than that of the working fluid in the gas phase, the contribution from heat conduction at the liquid-gas interface cannot be neglected in the thermal analysis of heat transfer in a heat pipe.

Conflict of interest

There is no conflict of interest.

Statement of significance

The ability to accurately predict thermal conductance (or its inverse thermal resistance) at liquid-gas interfaces is important for the study of evaporation of liquid droplets and the thermal analysis of various types of heat pipes. A good understanding of heat transfer mechanisms at liquid-gas interfaces can help design heat pipes with optimized cooling performance. In spite of its importance, the studies on thermal resistance at liquid-gas interfaces are rare. In this work, we used both theoretical analyses and molecular dynamics simulations to study heat transfer across liquid-gas interfaces. For all cases studied, the theoretical predictions agree with the MD simulation results very well. Our analyses show that if the density of the non-condensable gas is much higher than that of the working fluid in the gas phase, the contribution from heat conduction at the liquid-gas interface cannot be neglected in the thermal analysis of heat transfer in a heat pipe.

Acknowledgements

This work was supported by Edison International. We would also like to thank eXtreme Science and Engineering Discovery Environment (XSEDE) for providing us supercomputer resources for MD simulations.

References

[1] E.T. Swartz, R.O. Pohl, Rev. Mod. Phys. 61 (1989) 605.
[2] P.L. Kapitza, J. Phys. (USSR) 4 (1941) 181.
[3] D.G. Cahill, W.K. Ford, K.E. Goodson, G.D. Mahan, A. Majumda, H.J. Maris, R. Merlin, S.R. Phillpot, J. Appl. Phys. 93 (2003) 793.
[4] D.G. Cahill, P.V. Braun, G. Chen, D.R. Clarke, S. Fan, K.E. Goodson, P. Keblinski, W.P. King, G.D. Mahan, A. Majumdar, H.J. Maris, S.R. Phillpot, E. Pop, L. Shi, Appl. Phys. Rev. 1 (2014) 011305.
[5] Z. Liang, M. Hu, J. Appl. Phys. 123 (2018) 191101.
[6] G. Fang, C.A. Ward, Phys. Rev. E 59 (1999) 417.
[7] E.Y. Gatapova, I.A. Graur, O.A. Kabov, V.M. Aniskin, M.A. Filipenko, F. Sharipov, L. Tadrist, Int. J. Heat Mass Transfer 104 (2017) 800.
[8] Z. Liang, P. Keblinski, J. Chem. Phys. 148 (2018) 064708.
[9] F.O. Goodman, H.Y. Wachman, Dynamics of Gas-Surface Scattering, Academic, New York, 1976, pp. 23–31.
[10] Z. Liang, W. Evans, T. Desai, P. Keblinski, Appl. Phys. Lett. 102 (2013) 061907.
[11] Z. Liang, W. Evans, P. Keblinski, Phys. Rev. E 87 (2013) 022119.
[12] Z. Liang, P. Keblinski, Int. J. Heat Mass Transfer 78 (2014) 161.
[13] Z. Liang, T. Biben, P. Keblinski, Int. J. Heat Mass Transfer 114 (2017) 105.
[14] J. Yu, H. Wang, Int. J. Heat Mass Transfer 55 (2012) 1218.
[15] R.W. Schrage, A Theoretical Study of Interphase Mass Transfer, Columbia University Press, New York, 1953.
[16] V.P. Carey, Liquid-Vapor Phase-Change Phenomena, Hemisphere Publishing House, New York, 1992.
[17] S.C. Saxena, R.K. Joshi, Thermal Accommodation and Adsorption Coefficients of Gases, Hemisphere Publishing Corporation, New York, 1989.
[18] S.M. Foiles, M.I. Baskes, M.S. Daw, Phys. Rev. B 33 (1986) 7983.
[19] G.C. Maitland, M. Rigby, E.B. Smith, W.A. Wakeham, Intermolecular Forces: Their Origin and Determination, Clarendon Press, Oxford, 1981.
[20] A.K. Rappe, C.J. Casewit, K.S. Colwell, W.A. Goddard, W.M. Skiff, J. Am. Chem. Soc. 114 (1992) 10024.
[21] D. Frenkel, B. Smit, Understanding Molecular Simulation, Academic Press, San Diego, 2002, p. 75.
[22] P. Jund, R. Jullien, Phys. Rev. B 59 (1999) 13707.
[23] I.M.J.J. van de Ven-Lucassen, T.J.H. Vlugt, A.J.J. van der Zenden, P.J.A.M. Kerkhof, Mol. Phys. 94 (1998) 495.
[24] S. Srinivasan, R.S. Miller, Num. Heat Transfer, Part B 52 (2007) 297.
[25] Y. Chen, J. Chem. Phys. 124 (2006) 054113.
[26] R. Meland, Phys. Fluids 15 (2003) 3244.
[27] O. Wilhelmsen, T.T. Trinh, A. Lerik, Phys. Rev. E 97 (2018) 012126.
[28] Y.A. Cengel, A.J. Ghajar, Heat and Mass Transfer, Fundamentals & Applications, fifth ed. in SI units, McGraw Hill Education, 2014, pp. 864–866.
[29] E.L. Cussler, Diffusion: Mass Transfer in Fluid Systems, second ed., Cambridge University Press, New York, 1997.